

Decay and recurrence of non-Gaussian correlations in a quantum many-body system

Thomas Schweigler,¹ Marek Gluza,² Mohammadamin Tajik,¹ Spyros Sotiriadis,³ Federica Cataldini,¹ Si-Cong Ji,¹ Frederik S. Møller,¹ João Sabino,^{1,4,5} Bernhard Rauer,^{1,6} Jens Eisert,² and Jörg Schmiedmayer¹

¹Vienna Center for Quantum Science and Technology, Atominstitut, TU Wien, Stadionallee 2, 1020 Vienna, Austria

²Dahlem Center for Complex Quantum Systems, Freie Universität Berlin, 14195 Berlin, Germany

³Faculty of Mathematics and Physics, University of Ljubljana, Jadranska 19, SI-1000 Ljubljana, Slovenia

⁴Instituto de Telecomunicações, Physics of Information and Quantum Technologies Group, Av. Rovisco Pais 1, 1049-001, Lisbon, Portugal

⁵Instituto Superior Técnico, Universidade de Lisboa, Av. Rovisco Pais 1, 1049-001, Lisbon, Portugal

⁶Laboratoire Kastler Brossel, Ecole Normale Supérieure, Collège de France,

CNRS UMR 8552, Sorbonne Université, 24 rue Lhomond, 75005 Paris, France

(Dated: February 28, 2022)

Gaussian models provide an excellent effective description of a plethora of quantum many-body systems ranging from a large variety of condensed matter systems [1, 2] all the way to neutron stars [3]. Gaussian states are common at equilibrium when the interactions are weak. Recently it was proposed that they can also emerge dynamically from a non-Gaussian initial state evolving under non-interacting dynamics [4–11]. In this work, we present the first experimental observation of such a dynamical emergence of Gaussian correlations in a quantum many-body system. For this, we monitor the connected fourth-order correlations [12] during non-equilibrium dynamics. These dynamics are triggered by abruptly switching off the effective interaction between the collective degrees of freedom that we observe, while leaving the interactions between the microscopic constituents unchanged. Starting from highly non-Gaussian correlations, we observe a Gaussian description becoming increasingly accurate over time. In our closed system with non-interacting effective degrees of freedom, we do not expect full thermalization [13–19]. This memory of the initial state is confirmed by observing recurrences [20] of non-Gaussian correlations. Our study points to a natural way for Gaussian models to emerge in a wide class of (microscopically interacting) quantum many-body systems.

An ideal model to study the emergence of Gaussian states is the sine-Gordon model [21], which can be quantum simulated [22, 23] by two tunnel-coupled one-dimensional (1D) superfluids [24]. Changing the tunnel-coupling one can switch from an effectively strongly correlated system with non-Gaussian correlations [12] to weakly or even non-interacting effective degrees of freedom. The ability to change the tunneling, therefore, enables us to perform a sudden quench [25] in the interaction strength of the effective model.

In our experimental system, the superfluids are realized with ultracold bosons (⁸⁷Rb atoms) trapped in a double-well potential on an atom chip [26]. The double-well is created through dressing with radio frequency magnetic fields [27]. The height of the double-well barrier can be tuned by changing the amplitude of this dressing fields, thus allowing for different tunneling rates between the wells. Using matter-wave interference, we can extract the spatially resolved phase dif-

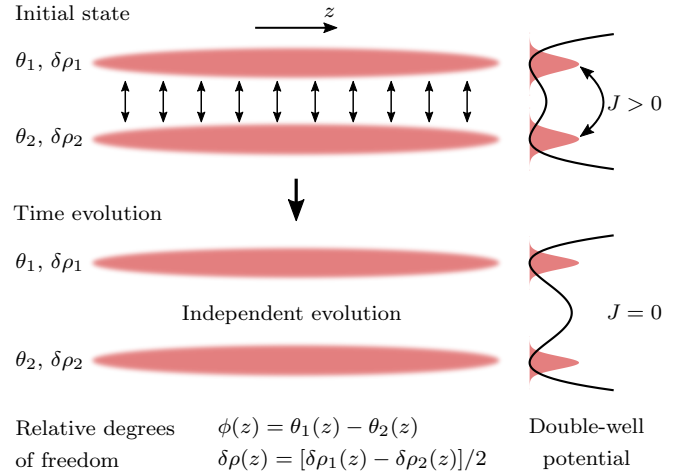


FIG. 1. Schematic of the experimental procedure. We investigate the non-equilibrium dynamics of two 1D superfluids in a double-well potential. Each of the superfluids is described through the density fluctuations $\delta\rho_{1,2}(z)$ around their common mean density profile $n_{1D}(z)$ as well as their phase fluctuations $\theta_{1,2}(z)$. From the quantities for the single superfluids, we define the relative phase fluctuations $\phi(z)$ and the relative density fluctuations $\delta\rho(z)$ as the respective differences. We initially prepare the system through evaporative cooling in a double-well potential with tunneling. Employing a slow cooling rate, we aim at creating a thermal equilibrium state. Subsequently, we switch off the tunneling J by ramping up the barrier separating the two wells and investigate the independent time evolution of the two superfluids.

ference $\phi(z)$ between the superfluids. We use a harmonic or a box-like trap for the 1D confinement of the superfluids. A schematics of the experimental system and the quench procedure (see discussion in the following paragraphs) is depicted in fig. 1.

As discussed in ref. [12], we can prepare states with distinctly non-Gaussian fluctuations of the relative phase $\phi(z)$ between the superfluids through slow evaporative cooling (aiming to create a thermal equilibrium state) in the double-well potential with tunneling. We found that the phase correlations of such states can be well described by the thermal

fluctuations of the sine-Gordon model

$$H_{\text{SG}} = \int dz \left[g_{1\text{D}}(z) \delta\rho^2(z) + \frac{\hbar^2 n_{1\text{D}}(z)}{4m} \left(\frac{\partial\varphi(z)}{\partial z} \right)^2 - 2\hbar J n_{1\text{D}}(z) \cos(\varphi(z)) \right] \quad (1)$$

in the classical field approximation. In addition to the relative phase fluctuations $\varphi(z)$, the Hamiltonian also contains the conjugate field, the relative density fluctuations $\delta\rho(z)$. In eq. (1), m represents the mass of the ^{87}Rb atoms, $n_{1\text{D}}(z)$ the 1D mean density profile, $g_{1\text{D}}(z)$ the 1D interaction strength, and J the single particle tunneling rate. Note that eq. (1) is an effective model, representing a low energy approximation of the interacting microscopic Hamiltonian [24].

The degree of non-Gaussianity of the state prepared by evaporative cooling depends on the phase-locking (higher for larger tunneling) between the superfluids. We quantify the phase-locking strength by the coherence factor $\langle \cos(\varphi) \rangle$. For very weak ($\langle \cos(\varphi) \rangle \approx 0$) and very strong phase-locking ($\langle \cos(\varphi) \rangle \approx 1$) the fluctuations follow a Gaussian distribution, while for intermediate phase-locking we observe non-Gaussian states. In our experimental protocol we start from such a non-Gaussian state and subsequently switch off the tunneling by ramping up the double-well barrier in approximately 2 ms. Afterwards, the two superfluids evolve independently in the double-well without tunneling. This corresponds to free evolution of the collective degrees of freedom $\varphi(z)$ and $\delta\rho(z)$ according to eq. (1) with $J = 0$ (see discussion of the theoretical model below). During the evolution, the relative phase is measured. Since the measurement procedure is destructive, only one spatially resolved phase profile at a certain evolution time is recorded per experimental realization.

From the extracted relative phase profiles $\varphi(z)$, we calculate correlation functions using the same procedure as was used in ref. [12]. Note that only phase differences between two spatial points are defined unambiguously. Therefore, we reference the phase to the center of the superfluid and calculate correlation functions of $\tilde{\varphi}(z) = \varphi(z) - \varphi(0)$. The N -th order equal-time phase correlation function is defined as

$$G^{(N)}(\mathbf{z}, t) = \langle \tilde{\varphi}(z_1, t) \dots \tilde{\varphi}(z_N, t) \rangle, \quad (2)$$

where the expectation value is calculated by averaging over many experimental realizations. The full correlation function, $G^{(N)}$, can be decomposed into [28]

$$G^{(N)}(\mathbf{z}, t) = G_{\text{dis}}^{(N)}(\mathbf{z}, t) + G_{\text{con}}^{(N)}(\mathbf{z}, t). \quad (3)$$

The first term, $G_{\text{dis}}^{(N)}$, is the *disconnected* part of the correlation function. It is fully determined by *all* the lower-order correlation functions, $G^{(N')}$ with $N' < N$, and therefore does not contain new information at order N . The second term, $G_{\text{con}}^{(N)}$, is the *connected* part of the correlation function, and contains genuine new information about the system at order N . An explicit formula for $G_{\text{con}}^{(N)}$ is given in the methods.

For Gaussian states, all higher-order correlations, $G^{(N)}$ with $N > 2$, fully factorize, i.e., all $G_{\text{con}}^{(N)}$ for $N > 2$ vanish. As a measure of non-Gaussianity of the relative phase fluctuations, we calculate the relative size of the fourth-order connected correlation function,

$$M^{(4)}(t) = \frac{S_{\text{con}}^{(4)}(t)}{S_{\text{full}}^{(4)}(t)} = \frac{\sum_{\mathbf{z}} |G_{\text{con}}^{(4)}(\mathbf{z}, t)|}{\sum_{\mathbf{z}} |G^{(4)}(\mathbf{z}, t)|}. \quad (4)$$

A non-zero value of this quantity implies that the fourth-order correlation function is not determined by the second moments via Wick's theorem [28]. Note that the experimental z -values lie on a discrete grid with a spacing of approximately $2 \mu\text{m}$, which is determined by the pixel-size of the camera used for absorption imaging. The sums in eq. (4) run over all distinct combinations of z_1, \dots, z_4 contained in a central interval of the superfluids.

The experimental results for the time evolution of $M^{(4)}$ as well as $S_{\text{full}}^{(4)}$ and $S_{\text{con}}^{(4)}$ are presented in fig. 2. We observe a fast decrease in $M^{(4)}$ driven by an increase in the magnitude of the phase fluctuations (increase in $S_{\text{full}}^{(4)}$) and a decrease in the fourth-order connected correlation functions (decrease in $S_{\text{con}}^{(4)}$). Considering the finite experimental statistics, the resulting final state is indistinguishable from Gaussian fluctuations. The Gaussian model that we compare with in the figures is simply given by the experimental mean values $\langle \tilde{\varphi}(z, t) \rangle$ and covariance matrix $\langle \tilde{\varphi}(z, t) \tilde{\varphi}(z', t) \rangle$ at the particular evolution time t . Note that the increase in the overall fluctuations corresponds to a decrease in the integrated interference contrast as previously observed [13, 14, 20] and can be explained by dephasing of non-interacting eigenmodes [29, 30]. Additional measurements for different initial phase-locking strengths show similar behavior (see the supplementary information).

Let us now discuss our theoretical model in more detail. As already mentioned above, we know that numerous aspects of the relative phase fluctuations of the initial state can be well described by the thermal fluctuations of the sine-Gordon model (1) in classical fields approximation [31]. We therefore use it for both the initial relative density and phase fluctuations. Our model for the initial state, therefore, leads to non-Gaussian phase fluctuations whose magnitude gets suppressed with increased tunneling. The non-Gaussianity is a direct consequence of the beyond quadratic tunneling term in H_{SG} (last term in eq. (1)). The suppression with increased tunneling can be understood from an energy argument and is explicitly discussed in the supplementary information. Meanwhile, the density fluctuations are Gaussian and independent of the tunneling rate since there is only a quadratic, J independent term of $\delta\rho$ in H_{SG} . Cross-correlations between density and phase fluctuations vanish since there are no cross terms in eq. (1).

For the time evolution we simply set J in eq. (1) to zero giving the Luttinger liquid model. As already discussed, this is a non-interacting model for the collective degrees of freedom, the relative phase and density fluctuations. The quadratic ef-

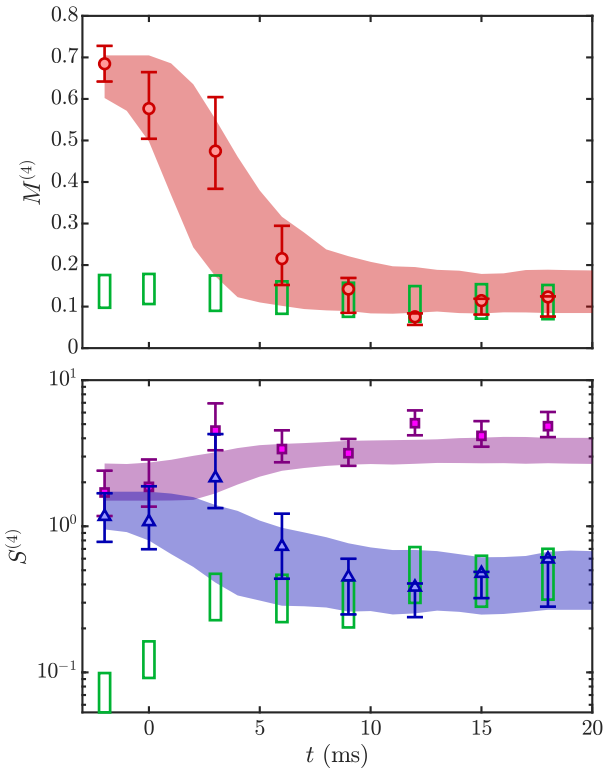


FIG. 2. Time evolution of the relative size of the fourth-order connected correlation functions. The experimental results for the measure $M^{(4)}$ (upper plot, red bullets) as well as for $S_{\text{full}}^{(4)}$ (lower plot, purple squares) and $S_{\text{con}}^{(4)}$ (lower plot, blue triangles) are shown as a function of the evolution time, t . The first point at $t = -2$ ms represents the initial state with a coherence factor $\langle \cos(\varphi) \rangle_{\text{init}} = 0.74$. Between $t = -2$ and 0 ms, the amplitude of the dressing fields is ramped up, leading to a decoupling of the two wells. The shaded area represents the theory prediction for the respective quantities, considering the finite statistics and uncertainty in the decoupling time (between -2 and 0 ms), but not the uncertainty in the initial thermal coherence length, λ_T , and single particle tunneling rate J (see Methods). The green rectangles represent the predictions for $M^{(4)}$ (upper subplot) and $S_{\text{con}}^{(4)}$ (lower subplot) following from Gaussian fluctuations considering the finite experimental sample size. All error bars as well as the vertical extension of the shaded areas and green rectangles represent 80% confidence intervals. We used bootstrapping to calculate the confidence intervals for the experimental data. The horizontal extension of the green rectangles was chosen arbitrarily. The experimental results have been obtained for a harmonic 1D trapping potential. The central $50\text{ }\mu\text{m}$ of the system are analyzed in experiment and theory, with the experimental system length being roughly $120\text{ }\mu\text{m}$.

ffective Hamiltonian can be diagonalized in terms of its eigenmodes. We get

$$\tilde{\varphi}_n(t) = \tilde{\varphi}_n(0) \cos(\epsilon_n t / \hbar) - C_n \delta \tilde{\rho}_n(0) \sin(\epsilon_n t / \hbar) \quad (5)$$

for the eigenmode expansion of the phase ($\tilde{\varphi}_n$) and density ($\delta \tilde{\rho}_n$) fluctuations. Here, we denote the eigenenergies by ϵ_n and C_n is a constant depending on the mode number n . From eq. (5), one can intuitively understand the experimental re-

sults. The large Gaussian density fluctuations of the initial state rotate into the phase quadrature while the small initial non-Gaussian phase fluctuations (suppressed by the tunneling) rotate out. This leads to a fast decrease in the relative size of the fourth-order connected correlation function. Note that the initial Gaussian density fluctuations are crucial for observing the dynamical emergence of Gaussian phase correlations in our model. In theory calculations with initial density fluctuations set to zero, a statistically significant fourth-order connected part remains at all times (see supplementary information).

The 1D mean density profile n_{1D} , and, as a consequence, also the 1D interaction strength g_{1D} (see Methods) might be position (z) dependent for a non-homogeneous system. The form of the eigenmodes, the eigenenergies ϵ_n and the constant C_n in eq. (5) depend on the form of this spatial dependencies (determined by the trapping geometry) and the choice of boundary conditions. A harmonic trapping potential leads to an incommensurate set of eigenenergies [32]. The different eigenmodes dephase with respect to each other leading to an apparent equilibration with the initial phase (density) fluctuations being distributed to both the phase and density quadratures [13, 29]. No rephasing is expected and the phase correlations should remain Gaussian after the initial dephasing.

For a homogeneous system on the other hand, the eigenenergies are equally spaced, the eigenmodes are given by sine and/or cosine functions depending on the boundary conditions. After an initial dephasing of the eigenmodes, we expect a rephasing at a later time with the system returning to its initial state. Indeed, we observed a recurrence of phase coherence in ref. [20] where a box-like confinement leading to a fairly homogeneous system was used. However, previously we only started from Gaussian initial states and did not investigate higher-order correlation functions. Using the same kind of confinement, but starting from a strongly non-Gaussian initial state, we now also observe a recurrence of non-Gaussian phase fluctuations as presented in fig. 3.

The experimental results presented in figs. 2 and 3 are in good agreement with the predictions of our theoretical model. Note that the evolution times presented in fig. 2 are rather short compared to the system size. Therefore, the exact trapping geometry does not matter too much as long as we analyze the approximately homogeneous central part of the system only. For simplicity, we therefore perform the theory calculations presented in fig. 2 for a large homogeneous system in order to avoid any boundary effects. Meanwhile, the calculations shown in fig. 3 are done for a homogeneous system of the same length as the experimental box-like confinement and Neumann boundary conditions. This represents an ideal hard-walled box. Here, the boundary and finite size effects are crucial for correctly describing the recurrences.

Our theoretical explanation is related to former theoretical work [4–11] in the sense that it relies on the dephasing of non-interacting eigenmodes. However, previously, the emergence of Gaussian correlations due to spatial mixing of the initial correlation functions has been discussed. Such a process alone

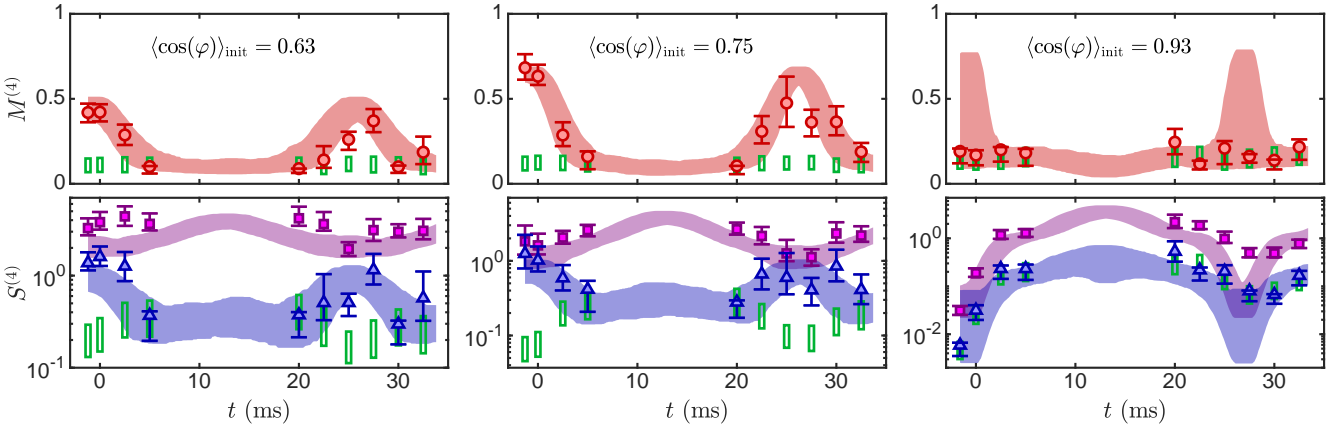


FIG. 3. **Recurrence of the non-Gaussian phase fluctuations.** As for fig. 2, but for a $50\text{ }\mu\text{m}$ long near-homogeneous system (box-like 1D confinement) and several different initial phase-locking strengths quantified by $\langle \cos(\varphi) \rangle_{\text{init}}$. In all cases a recurrence of coherence [20] can be observed around 25 ms, indicated by a dip in the value of $S_{\text{full}}^{(4)}$. In the measurements with $\langle \cos(\varphi) \rangle_{\text{init}} = 0.63$ or 0.75, the initial state exhibits non Gaussian phase correlations, and we also observe a recurrence in the relative ($M^{(4)}$) and absolute ($S_{\text{con}}^{(4)}$) size of the connected fourth-order correlation function. In the measurement with $\langle \cos(\varphi) \rangle_{\text{init}} = 0.93$, the initial phase fluctuations are Gaussian, and no such peak in $M^{(4)}$ occurs. This supports the picture that the recurrences of non-Gaussian fluctuations are due to memory of the initial state being preserved. The central $38\text{ }\mu\text{m}$ of the system are analyzed in experiment and theory.

cannot explain our experimental results. For a correct description, our theoretical model relies on the mixing between the two quadratures (phase and density fluctuations) and the properties of the initial state. We believe that the observed mechanism could also be relevant for various other physical systems and experimental protocols.

In addition to dephasing, further equilibration might occur in our system due to additional terms beyond second order not considered in the low energy effective model stated in eq. (1). Such terms lead to the damping of the recurrence heights observed in ref. [20]. We expect that the additional terms also lead to a damping of the recurrences of $M^{(4)}$ when investigating longer evolution times or bigger sample sizes. The investigation of such a damping will be the objective of future studies. We believe that the experimental setting laid out here has the potential to provide these and related insights into the study of interacting quantum matter in non-equilibrium scenarios [18, 19], tackling long-standing questions at the interface of statistical mechanics and microscopic quantum many-body physics.

METHODS

Details of the experimental realization

The (tunnel-coupled) 1D superfluids are realized using ultracold gases of ^{87}Rb in a double-well potential on an atom chip [26]. Each well consists of a highly elongated cigar-shaped trap (two tightly confined directions, one direction with weak confinement, corresponding to the 1D direction z). The wells are separated along one of the tightly confined directions (see fig. 1). The separation is horizontal, avoiding the

influence of gravity. By tuning the height of the barrier separating the wells we can change the tunnel-coupling between the two superfluids.

The clouds are initially prepared by evaporatively cooling the atoms whilst keeping the double-well trap static. The relative evaporation rates at the end of the cooling ramp amount to a few percent per 10 ms. Right after the end of the evaporative cooling, the double-well barrier is ramped up to start the non-equilibrium evolution (see discussion in the main text and fig. 1).

The measured harmonic frequency for the weakly confined direction is $\omega_z \approx 2\pi \times 7\text{ Hz}$, leading to clouds of approximately $120\text{ }\mu\text{m}$ length. In addition to this harmonic magnetic confinement we superimpose a box-shaped optical potential for some of the measurements. For the results presented in fig. 3, the optical potential was created by a laser with 660 nm wavelength (blue detuned) and shaped by a digital micromirror device (DMD) [33]. For the measurements presented in the supplementary information, a 767 nm (blue detuned) laser was used together with a simple mask [20, 34].

Calculation of the correlation functions and their connected parts

As defined in eq. (2) in the main text, we evaluate the phase correlation functions as

$$G^{(N)}(\mathbf{z}, t) = \langle [\varphi(z_1, t) - \varphi(0, t)] \dots [\varphi(z_N, t) - \varphi(0, t)] \rangle,$$

where the brackets denote the averaging over different experimental realizations and $\varphi(z)$ is extracted via matter-wave interference. Similarly, we calculate the connected part us-

ing [35]

$$G_{\text{con}}^{(N)}(\mathbf{z}, t) = \sum_{\pi} \left[(|\pi| - 1)! (-1)^{|\pi|-1} \prod_{B \in \pi} \left\langle \prod_{i \in B} [\varphi(z_i, t) - \varphi(0, t)] \right\rangle \right]. \quad (6)$$

Here the sum runs over all possible partitions π of $\{1, \dots, N\}$, the first (left) product runs over all blocks B of the partition and the second (right) product runs over all elements i of the block. $|\pi|$ is the number of blocks in the partition. Note that eq. (6) does not represent an unbiased estimator of the connected correlation function. However, for our large sample sizes the bias should be negligible.

Details of the theory calculation

The theoretical calculations are performed numerically. Moreover, a homogeneous system is assumed. For sampling the phase fluctuations of the initial state (thermal fluctuations of the sine-Gordon model), we use the method discussed in refs. [12, 31]. This method produces numerical realizations of a certain length, which represents a part of an infinite system. The thermal fluctuations for the sine-Gordon model in classical fields approximation are determined by the thermal coherence length, λ_T , and the single particle tunneling rate, J [12, 36]. Self consistently fitting both λ_T and J from the initial state is very challenging since the parameters are correlated for the attempted fitting procedures [37]. In order to avoid overfitting or large fitting errors, we use $\lambda_T = 11 \mu\text{m}$ as a reasonable value for all theoretical calculations presented in the paper and supplementary information. Having set the value of λ_T , we self consistently fit J from the initial values of $\langle \cos(\varphi) \rangle$ leading to the different values of J used in the theory calculations for the different measurements. The experimental value of $\langle \cos(\varphi) \rangle_{\text{init}}$ used for the fit is obtained by averaging over the experimental realizations as well as the same central interval of the superfluids used also for all other analysis. Note that both the evolution of $M^{(4)}$ and $S_{\text{con}}^{(4)}$ is rather insensitive to the value of λ_T . In other words, the conclusions concerning the dynamical emergence of Gaussian correlations and the recurrence of non-Gaussian correlations are insensitive to the particular choice of λ_T . In contrast, the evolution of $S_{\text{full}}^{(4)}$ strongly depends on λ_T . Given our choice of λ_T , the experimental results and theory predictions for $S_{\text{full}}^{(4)}$ agree fairly well in most cases.

Numerical sampling of the thermal density fluctuations is straightforward as the fluctuations are Gaussian. The thermal density fluctuations for the sine-Gordon model in classical fields approximation are determined by the 1D interaction strength, $g_{1\text{D}}$, and again by the thermal coherence length, λ_T . We use the density broadened 1D interaction

strength [20, 34, 37]

$$g_{1\text{D}} = \hbar \omega_{\perp} a_s \frac{2 + 3a_s n_{1\text{D}}}{(1 + 2a_s n_{1\text{D}})^{3/2}}, \quad (7)$$

for both the initial state and the time evolution. In eq. (7), $a_s = 5.2 \mu\text{m}$ [38] is the 3D scattering length. The transverse trapping frequency is $\omega_{\perp} = 2\pi \times 1.4 \text{ kHz}$ for the results presented in fig. 2 and the supplementary information. For fig. 3 on the other hand, we use $\omega_{\perp} = 2\pi \times 1.45 \text{ kHz}$. For the homogeneous 1D atomic density, $n_{1\text{D}}$, we use the value averaged over the analyzed central part of the superfluids.

Having obtained numerical realizations for the initial state, we numerically evolve them with the discretized version of eq. (1) and $J = 0$. We use Neumann boundary conditions and a homogeneous system, i.e., a constant $n_{1\text{D}}$ and $g_{1\text{D}}$. For the results presented in fig. 2 and the supplementary information, we use a theoretical system size of $L = 200 \mu\text{m}$. Therefore, as desired, we do not get any influence of the boundaries for the investigated time scales in the central part of the system. The outcome mimics the results for an infinite system. For the theory predictions presented in fig. 3, we use the actual length $L = 50 \mu\text{m}$ of the experimental system.

In order to correctly consider the effect of the finite experimental sample size, we set the number of numerical realizations equal to the experimental sample size of the corresponding measurements. The experimental sample sizes vary between 118 and 623 (median 390) for the different measurements. The calculations are then repeated 200 times to obtain the confidence intervals presented in the figures.

For all presented theory predictions, the effect of the finite experimental spatial resolution is approximated by convolving the numerically calculated phase profiles with a Gaussian of a standard deviation of $\sigma_{\text{PSF}} = 3 \mu\text{m}$ [37] before calculating the presented quantities.

ACKNOWLEDGMENTS

We thank Igor Mazets, Sebastian Erne, Thomas Gasenzer, Jürgen Berges and Tim Langen for helpful discussions. This work is supported by the ERC Advanced Grant “QuantumRelax”, the DFG Collaborative Research Centre “SFB 1225 (ISOQUANT)”, and the JTF project “The Nature of Quantum Networks” (ID 60478). J.E. acknowledges funding from the DFG (FOR 2724, EI 519/9-1, EI 519/7-1, CRC 183), the FQXi, and the European Union’s Horizon 2020 research and innovation programme under grant agreement No 817482 (PASQuanS). F.C., F.M., B.R., J.Sa., and T.S. acknowledge support by the Austrian Science Fund (FWF) in the framework of the Doctoral School Complex Quantum Systems (CoQuS). S.S. acknowledges support by the Slovenian Research Agency (ARRS) under grant QTE (N1-0109) and by the ERC Advanced Grant OMNES (694544). J.Sa. acknowledges support by the Fundação para a Ciência e a Tecnologia (PD/BD/128641/2017). J.E., M.G., and S.S. would

like to thank the Erwin Schrödinger Institute for its hospitality and support under the programme “Quantum Simulation - from Theory to Application” (LCW 2019). S.J. acknowledges supported by the European Union’s Horizon 2020 research and innovation program under the Marie Skłodowska-Curie grant agreement No. 801110 (“1D-AGF”) through an Erwin Schrödinger Quantum Science & Technology (ESQ) Fellowship.

AUTHOR CONTRIBUTIONS

T.S. performed the experiment and data analysis with contributions by M.T., B.R., F.C., S.J., F.M., and J.Sa. T.S. did the theory calculations with contributions by M.G. and S.S. J.Sch. and J.E. provided scientific guidance in experimental and theoretical questions. J.Sch. conceived the experiment. All authors contributed to the interpretation of the data and to the writing of the manuscript.

[1] S. M. Girvin and K. Yang, *Modern condensed matter physics* (Cambridge University Press, Cambridge).

[2] A. Altland and B. D. Simons, *Condensed Matter Field Theory*, 2nd ed. (Cambridge University Press, 2010).

[3] S. Gandolfi, A. Gezerlis, and J. Carlson, *Ann. Rev. Nucl. Part. Sc.* **65**, 303 (2015).

[4] R. Haag, R. Kadison, and D. Kastler, *Commun. Math. Phys.* **33**, 1 (1973).

[5] M. Cramer, C. M. Dawson, J. Eisert, and T. J. Osborne, *Phys. Rev. Lett.* **100**, 030602 (2008).

[6] M. Cramer and J. Eisert, *New J. Phys.* **12**, 055020 (2010).

[7] S. Sotiriadis and P. Calabrese, *J. Stat. Mech.: Theory Exp.* **2014**, P07024 (2014).

[8] M. Gluza, J. Eisert, and T. Farrelly, *SciPost Phys.* **7**, 38 (2019).

[9] C. Murthy and M. Srednicki, *Phys. Rev. E* **100**, 012146 (2019).

[10] T. Monnai, S. Morodome, and K. Yuasa, *Phys. Rev. E* **100**, 022105 (2019).

[11] T. Ishii and T. Mori, *Phys. Rev. E* **100**, 012139 (2019).

[12] T. Schweigler, V. Kasper, S. Erne, I. Mazets, B. Rauer, F. Cataldini, T. Langen, T. Gasenzer, J. Berges, and J. Schmiedmayer, *Nature* **545**, 323 (2017).

[13] M. Gring, M. Kuhnert, T. Langen, T. Kitagawa, B. Rauer, M. Schreitl, I. E. Mazets, D. Adu Smith, E. Demler, and J. Schmiedmayer, *Science* **337**, 1318 (2012).

[14] T. Langen, R. Geiger, M. Kuhnert, B. Rauer, and J. Schmiedmayer, *Nat. Phys.* **9**, 640 (2013).

[15] T. Langen, S. Erne, R. Geiger, B. Rauer, T. Schweigler, M. Kuhnert, W. Rohringer, I. E. Mazets, T. Gasenzer, and J. Schmiedmayer, *Science* **348**, 207 (2015).

[16] M. Schreiber, S. S. Hodgman, P. Bordia, H. P. Lüschen, M. H. Fischer, R. Vosk, E. Altman, U. Schneider, and I. Bloch, *Science* **349**, 842 (2015).

[17] P. Calabrese, F. H. L. Essler, and M. Fagotti, *Phys. Rev. Lett.* **106**, 227203 (2011).

[18] A. Polkovnikov, K. Sengupta, A. Silva, and M. Vengalattore, *Rev. Mod. Phys.* **83**, 863 (2011).

[19] J. Eisert, M. Friesdorf, and C. Gogolin, *Nat. Phys.* **11**, 124 (2015).

[20] B. Rauer, S. Erne, T. Schweigler, F. Cataldini, M. Tajik, and J. Schmiedmayer, *Science* **360**, 307 (2018).

[21] J. Cuevas-Maraver, P. G. Kevrekidis, and F. Williams, eds., *The sine-Gordon model and its applications*, Nonlinear systems and complexity (Springer International Publishing, Switzerland, 2014).

[22] J. I. Cirac and P. Zoller, *Nat. Phys.* **8**, 264 (2012).

[23] I. Bloch, J. Dalibard, and S. Nascimbène, *Nat. Phys.* **8**, 267 (2012).

[24] V. Gritsev, A. Polkovnikov, and E. Demler, *Phys. Rev. B* **75**, 174511 (2007).

[25] P. Calabrese and J. Cardy, *Phys. Rev. Lett.* **96**, 136801 (2006).

[26] J. Reichel and V. Vuletić, eds., *Atom Chips* (Wiley-VCH, Weinheim, Germany, 2011).

[27] T. Schumm, S. Hofferberth, L. M. Andersson, S. Wildermuth, S. Groth, I. Bar-Joseph, J. Schmiedmayer, and P. Krüger, *Nat. Phys.* **1**, 57 (2005).

[28] J. Zinn-Justin, *Quantum Field Theory and Critical Phenomena*, 4th ed., International Series of Monographs on Physics (Clarendon Press, Oxford, 2002).

[29] T. Kitagawa, A. Imambekov, J. Schmiedmayer, and E. Demler, *New J. Phys.* **13**, 073018 (2011).

[30] T. Langen, T. Schweigler, E. Demler, and J. Schmiedmayer, *New J. Phys.* **20**, 023034 (2018).

[31] S. Beck, I. E. Mazets, and T. Schweigler, *Phys. Rev. A* **98**, 023613 (2018).

[32] R. Geiger, T. Langen, I. E. Mazets, and J. Schmiedmayer, *New J. Phys.* **16**, 053034 (2014).

[33] M. Tajik, B. Rauer, T. Schweigler, F. Cataldini, J. Sabino, F. S. Møller, S.-C. Ji, I. E. Mazets, and J. Schmiedmayer, *Opt. Express* **27**, 33474 (2019).

[34] B. Rauer, *Non-equilibrium dynamics beyond dephasing: Recurrences and loss induced cooling in one-dimensional Bose gases*, Ph.D. thesis, TU Wien (2018).

[35] A. N. Shiryaev, *Probability-1*, 3rd ed., Graduate Texts in Mathematics, Vol. 95 (Springer, New York, 2016) p. 349.

[36] P. Grišins and I. Mazets, *Phys. Rev. A* **87**, 013629 (2013).

[37] T. Schweigler, *Correlations and dynamics of tunnel-coupled one-dimensional Bose gases*, Ph.D. thesis, TU Wien (2019), arXiv:1908.00422 [cond-mat.quant-gas].

[38] E. G. M. van Kempen, S. J. J. M. F. Kokkelmans, D. J. Heinzen, and B. J. Verhaar, *Phys. Rev. Lett.* **88**, 093201 (2002).

[39] S. Sotiriadis, *Phys. Rev. A* **94**, 031605 (2016).

[40] S. Sotiriadis, *J. Phys. A* **50**, 424004 (2017).

[41] M. Gluza et. al., (in preparation).

[42] N. Whitlock and I. Bouhoule, *Phys. Rev. A* **68**, 053609 (2003).

Supplementary Information

Additional experimental results

We performed experimental measurements for several different initial phase-locking strengths and different trapping geometries. The experimental results not shown in the main text are presented in fig. S1. In all cases we observe a sharp decrease in the relative size $M^{(4)}$ of the fourth-order connected correlation function similar to what was observed in fig. 2 of the main text. Note the different speeds for the decay observed in fig. S1. For stronger initial phase-locking we generally observe a faster decay. This is in accordance with our theoretical model. One can understand the trend by realizing that the phase-fluctuations of the initial state get smaller with increasing phase-locking and are therefore more quickly overshadowed by the mixed-in initial density fluctuations.

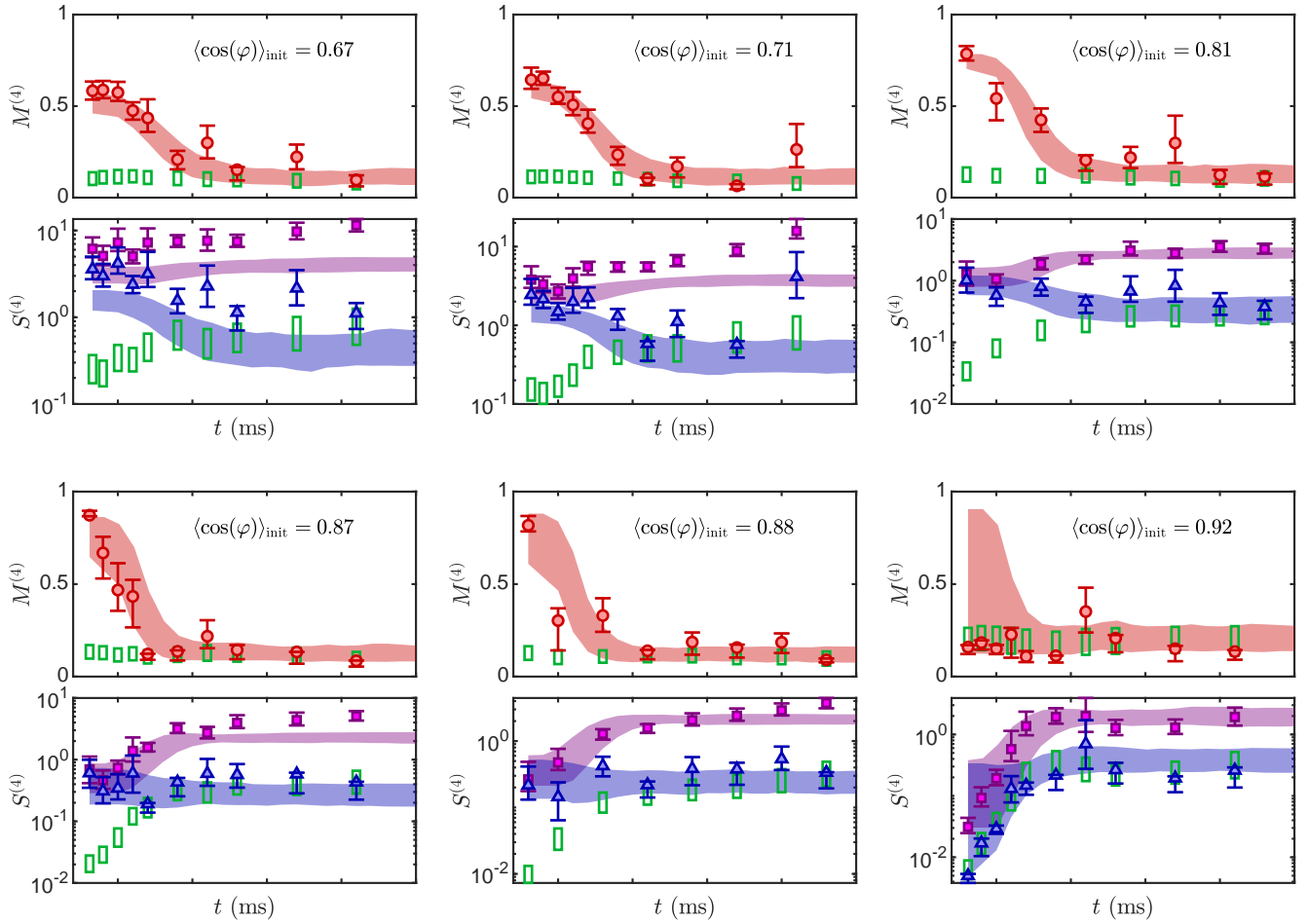


FIG. S1. **Time evolution of the relative size of the fourth-order connected correlation functions.** As for fig. 2, but for several different initial phase-locking strengths (quantified by $\langle \cos(\varphi) \rangle_{\text{init}}$) and different trapping geometries. The results for a $\langle \cos(\varphi) \rangle_{\text{init}}$ of 0.81 and 0.88 have been obtained with a harmonic confinement. For all other results, a 75 μm long box trap has been superimposed onto the harmonic confinement. We find that Gaussian correlations emerge dynamically for all measurements, independent of the initial phase-locking strength or the trapping geometry. The speed for the decay of $M^{(4)}$ increases with initial phase-locking in agreement with our theoretical model (see discussion in the text).

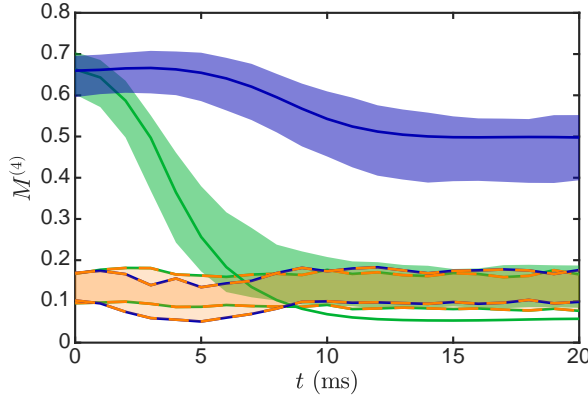


FIG. S2. Theory predictions with (green) and without (blue) initial density fluctuations. For the parameters of the measurement shown in fig. 2. The solid lines give the results for 10^5 numerical realizations while the shaded areas give the uncertainty considering the experimental sample size of 378. The orange shaded areas bounded by the dashed lines represent the predictions for Gaussian fluctuations. The green-orange and blue-orange dashed boundary lines mark the results for the case with and without initial density fluctuations respectively. As one can see, with initial density fluctuations, the final state appears Gaussian (assuming the experimental sample size) while the theory prediction without initial density fluctuations stays distinctively non-Gaussian.

Additional discussion of the theoretical model

Importance of the initial density fluctuations As already discussed in the main text, in our theoretical model, the dynamical emergence of Gaussian correlations is due to the rotating of large Gaussian fluctuations from the density to the phase quadrature. In order to illustrate this explicitly, we compare the theory predictions for the usual case with initial density fluctuations and the fictitious case of having no initial density fluctuations. As can be seen from fig. S2, a significant connected fourth-order correlation remains at all times for the theory calculation without initial density fluctuations, consistently with general theoretical predictions for Luttinger liquid dynamics [39, 40]. This observation demonstrates the crucial importance of the Gaussian initial density fluctuations for the dynamical emergence of Gaussian correlations, in our model. Note that also without initial density fluctuations the theory predicts a slight decrease in $M^{(4)}$ [41].

Relative size of the initial phase and density fluctuations Let us now explicitly show that in our theoretical model the initial phase fluctuations are suppressed compared to the initial density fluctuations. For the comparison of the two quantities, we have to consider the factor C_n from eq. (5), i.e., we want to compare $\langle \tilde{\varphi}_n^2(t=0) \rangle$ with $\langle C_n^2 \delta \tilde{\rho}_n^2(t=0) \rangle$. Remember that $\tilde{\varphi}_n$ and $\delta \tilde{\rho}_n$ represent the eigenmode expansions of the phase and density fluctuations respectively. Assuming a homogeneous system with Neumann boundary conditions, the eigenmodes are given by cosine functions. We get

$$C_n = \frac{2g_{1D}}{\hbar c k_n}, \quad (S1)$$

where k_n is the wavenumber taking the values

$$k_n = n \frac{\pi}{L} \quad (S2)$$

with n being a positive integer. The speed of sound is denoted by c and can be calculated as

$$c = \sqrt{\frac{g_{1D} n_{1D}}{m}}. \quad (S3)$$

In fig. S3 the results for the lowest non-zero mode ($k_1 = \pi/L$) are shown as a function of the phase-locking. We see that for the parameter range used in the experiment, the phase fluctuations are suppressed compared to the density fluctuations. For higher k_n this suppressing will get less. However, the integral quantities of eq. (4) will be dominated by the lowest lying modes.

Validity of the classical fields approximation Since the Heisenberg and Hamiltonian equations of motion are identical for conjugate fields, our discussion is reduced to the initial state. From the validity of the classical fields approximation for the thermal initial state directly follows that the initial density fluctuations are Gaussian, which is an important prerequisite of our proposed mechanism for the emergence of Gaussian phase correlations.

Using the classical fields approximation for a thermal state corresponds to making two approximations: Firstly, the quantum (zero temperature) fluctuations are neglected. Secondly, the Bose-Einstein distribution for the occupation of the eigenmodes

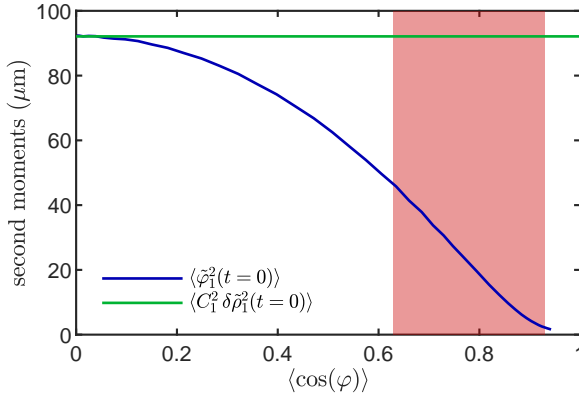


FIG. S3. Magnitude of the initial phase and density fluctuations in the theoretical model. Cosine transformed initial phase (blue line) and density (green line) fluctuations. The results for $k_1 = \pi/L$ are shown as a function of the phase locking strength. The system size $L = 50 \mu\text{m}$ is chosen to be consistent with fig. 3. The results for the phase fluctuations are obtained numerically (see discussion in the methods) while for the density fluctuations $\langle C_n^2 \delta \rho_n^2(t=0) \rangle = 4/(\lambda_T k_n^2)$ is used. As for all other presented theory calculations $\lambda_T = 11 \mu\text{m}$. The range of phase-locking used in the experiment is indicated by the red shaded area. The finite experimental spatial resolution is considered for $\langle \cos(\varphi) \rangle$ but not for the second moments.

is replaced by the Rayleigh-Jeans distribution. Both approximations are good when the thermal occupation of the eigenmodes under consideration is sufficiently large. Expressed as an equation the criteria read

$$\frac{1}{e^{\beta\epsilon_n} - 1} + \frac{1}{2} \approx \frac{1}{\beta\epsilon_n}, \quad (\text{S4})$$

which is fulfilled for small values of $\beta\epsilon_n$. Here $\beta = (k_B T)^{-1}$ and ϵ_n are the mode energies. Clearly the fulfillment of eq. (S4) depends on the mode-energy under consideration. For the discussion we will therefore consider the highest mode that can still be resolved in experimental measurements.

For simplicity, we will use the quadratic approximation [42]

$$H = \int dz \left[g_{1D}(z) \delta \rho^2(z) + \frac{\hbar^2 n_{1D}(z)}{4m} \left(\frac{\partial \varphi(z)}{\partial z} \right)^2 + \hbar J n_{1D}(z) \varphi^2(z) \right] \quad (\text{S5})$$

of eq. (1) for our discussion. Equation (S5) is a good approximation for large phase-locking and, trivially, for zero tunneling. Further assuming a homogeneous system, the eigenmodes are given by sine and/or cosine modes, depending on the boundary conditions. The eigenenergy for the wavenumber k is given by

$$\epsilon_n = \hbar c \sqrt{k^2 + \frac{1}{l_J^2}}. \quad (\text{S6})$$

Here l_J is the healing length of the relative phase, it can be calculated as

$$l_J = \sqrt{\frac{\hbar}{4mJ}}. \quad (\text{S7})$$

A sensible upper bound for k can be derived from the spatial resolution of the phase measurement, which in turn can be bounded by the pixel size, $\Delta z_{\text{pix}} = 2 \mu\text{m}$, of the used absorption imaging system. We therefore use $k = 2\pi/\Delta z_{\text{pix}}$ together with typical values for the temperature ($T = 70 \text{ nK}$) and speed of sound ($c = 1.8 \text{ mm/s}$). For the tunneling rate J , we use the highest experimental value leading to the lowest $l_J = 2 \mu\text{m}$. With this values the left and right hand side of eq. (S4) differ by only 3%, justifying the use of the classical field approximation. Even though our argument was demonstrated using the quadratic approximation, we expect it to remain valid for the sine-Gordon model since the higher modes, where quantum effects might be relevant, are not affected strongly by the tunneling term.